analytical chemistry

Article

pubs.acs.org/ac

Quantum Dot-Based Near-Infrared Electrochemiluminescent Immunosensor with Gold Nanoparticle-Graphene Nanosheet Hybrids and Silica Nanospheres Double-Assisted Signal Amplification

Jing Wang,[†] Heyou Han,*[,†] Xiaochun Jiang,[†] Liang Huang,[†] Lina Chen,[†] and Na Li[†]

[†]State Key Laboratory of Agricultural Microbiology, College of Science, Huazhong Agricultural University, Wuhan 430070, P.R. China

Supporting Information

ABSTRACT: Near-infrared electrochemiluminescence (NIR ECL) from quantum dots (QDs) has aroused particular attention. However, whether it is possible to achieve NIR ECL sensing has remained an open question. In this article, we reported a NIR ECL immunosensor with amplification techniques for ultrasensitive and selective determination of biomarker. In this sensing platform, NIR-emitting CdTe/CdS $core_{small}/shell_{thick}$ QDs were first selected as NIR ECL emitters. The NIR ECL nanoprobe (SiO_2-QD-Ab2) was designed by covalent assembly of goat antihuman IgG antibody (Ab2) on CdTe/CdS QDs tagged silica nanospheres. Gold nanoparticle-graphene nanosheet (Au-GN) hybrids were prepared by a sonication-induced self-assembly and served as an effective matrix for initial antibodies (Ab1) attachment. After a sandwich immunoreaction, the functionalized silica nanosphere labels were captured onto the glass carbon electrode surface. Integrating the dual amplification from the promoting electron transfer rate of Au-GN hybrids and the increasing QD loading of SiO_2-QD-Ab2 labels, the NIR ECL response from CdTe/CdS QDs enhanced 16.8-fold compared to the unamplified protocol and successfully fulfilled the ultrasensitive detection of human IgG (HIgG) with a detection limit of 87 fg mL^{-1}. Moreover, as a practical application, the proposed immunosensor was used to monitor HIgG level in human serum with satisfactory results obtained.

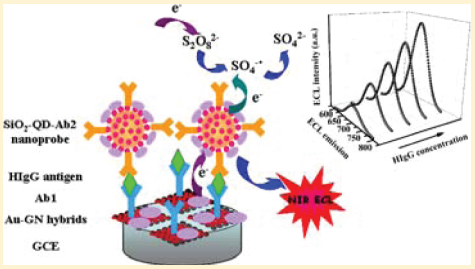

Quantum dots (QDs) emitting in the near-infrared (NIR) window, between 650 and 900 nm, have been extensively studied in some active fields, benefiting from their attractive advantages such as improved tissue penetration, lower background interference, and reduced photochemical damage.[1] Recent works have indicated the high-quality NIR-emitting QDs have potential applications for the use as fluorescent labels both in bioassays and bioimagings.[2] Despite NIR fluorescence could efficiently decrease the background signals in bioassays, the low photoluminescence quantum yield (PL QY) of NIR-emitting QDs and intrinsically low signal-to-noise ratio of fluorescent technique also impeded the improvement of detection sensitivity of target biomolecules.[2a,b] Therefore, further explorations on their superior emitting properties by different methods are of great importance.

As an alternative, electrochemiluminescence (ECL) is an attractive luminescent property for both fundamental study and analytical application of QDs. In recent years, ECL of II−VI QDs has been extensively studied and demonstrated that the QDs are electrically excitable in both organic[3] and aqueous media.[4] The reduced and oxidized ECL precursors, generated at some electrochemical potentials, can react with some coreactants such as $S_2O_8^{2-}$,[5] H_2O_2,[6] and O_2[7] to produce ECL in aqueous solution. Since the pioneering work concerning ECL sensors of CdSe QDs,[6a] the applications of QDs to ECL sensors have been paid tremendous attention and proven to be a new perspective for the use of QDs.[5,6b] However, the current QD-based ECL emitters for sensing, such as CdS,[5a] CdTe,[6b] and CdSe[5b] were mainly located in the visible range. The resulted high background would lead a lower signal-to-noise and/or cause interference with the detection. Most recently, with the development of synthetic strategies of NIR-emitting QDs, great efforts have been made toward the ECL studies from NIR-emitting QDs because of their promising NIR ECL property.[8] Unfortunately, the present reported work only focused on the fundamental properties and theoretical explanations of NIR ECL from QDs;[8a−d] rational design of biosensors based on the NIR ECL from QDs remains little explored in spite of the fact that the NIR window it offers in the sensor design of lower background interference.[8e] The reasons are mainly that the ECL emissions of present NIR-emitting QDs are relatively weak and unstable and the detectors of ECL instruments toward NIR luminescence are insensitive. Thus, the main challenges of moving QD-based ECL system from visible to NIR window are to find stable and strong NIR ECL emitters and then explore effective approaches to enhance NIR ECL.

Signal amplification is the most popular strategy that has been extensively used for the development of ultrasensitive immunoassay methods. The use of nanomaterials as signal

Received: February 20, 2012
Accepted: May 3, 2012
Published: May 3, 2012

   dx.doi.org/10.1021/ac300498v | *Anal. Chem.* 2012, 84, 4893−4899

Scheme 1. NIR ECL Immunoassay of HIgG with Dual Amplification Strategy

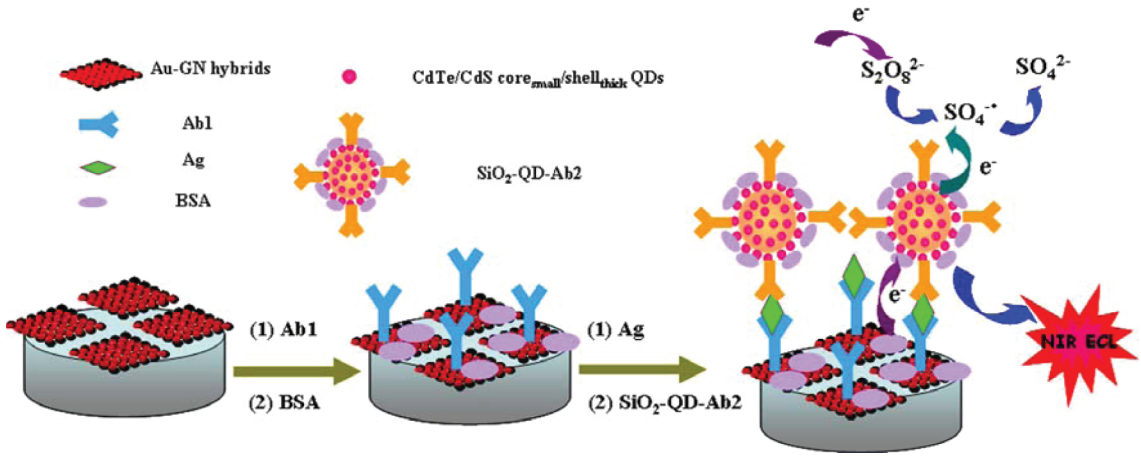

amplifiers is of particular interest in biosensor design, due to their outstanding optical, electronic, and biocompatible performance. Graphene nanosheet (GN) is a single layer of carbon atoms densely packed in a honeycomb crystal lattice which has attracted considerable research efforts from both experimental and theoretical communities in recent years owing to its excellent physical and electrical properties.[9] In particular, great progress has been made in creating metal nanoparticles (NPs)-GN hybrids by *in situ* decorating or assembling metal NPs on the GN.[10] Gold NPs-GN (Au-GN) hybrids have always been the subject of intense ECL study because of their good potential as enhanced substrates for ECL applications.[10c−e] On the other hand, to substitute a single label with a carrier loaded with a large number of labels is a versatile signal ampification technique widely used in ECL-based bioassay. It has been reported that silica (SiO_2) nanospheres are well recognized as commonly used nanocarriers because of their excellent water-solubility, simple surface functionalization, and good biocompatibility.[11] Taking into consideration the above advantages, it would be an effective way to integrate Au-GN hybrids with functionalized SiO_2 nanospheres as magnified elements for constructing sensitive NIR ECL biosensor with a particular analytical sensing design.

In this contribution, we first design and report a QD-based NIR ECL immunosensor for ultrasensitive protein detection by employing Au-GN hybrids and SiO_2 nanospheres for dual amplification. Here, we used the CdTe/CdS core$_{small}$/shell$_{thick}$ QDs as the NIR ECL emitters, instead of the new NIR ECL reagent previously reported by our group.[8c] Although the latter NIR-emitting CdTe/CdS QDs prepared by the hydrothermal method could produce successive NIR ECL, further work found the ECL intensity and stability recorded from as-prepared CdTe/CdS QDs were hard to meet the requirements of analytical applications, because they suffered from the strong interference of the abundant defects locating on the particle surface. In contrast, the "thick shell" model not only largely decreased the surface traps of present QDs but also highly improved their brightness and stability, providing the potential possibility as ECL emitters for NIR sensing. Scheme 1 describes the fabrication process of the NIR ECL immunosensor. The introduction of Au-GN hybrids accelerated the electron transfer rate to amplify the electrochemical signal as well as provided a biocompatible microenvironment for the immobilization of antibody. SiO_2 nanospheres were selected as nanocarriers for loading numerous CdTe/CdS core$_{small}$/shell$_{thick}$ QDs to form QDs tagged SiO_2 nanosphere labels and were brought onto the electrode surface upon the completion of sandwich immunoreactions. By coupling with the NIR window and ECL analytical technique, the present immunosensor showed an excellent analytical performance for the ultrasensitive detection of human IgG (HIgG) in both aqueous buffers and the serum samples.

EXPERIMENTAL SECTION

Reagents. Human IgG antigen (Ag, dry power), rabbit antihuman IgG antibody (Ab1, 1 mg mL^{-1}), and goat antihuman IgG antibody (Ab2, 1 mg mL^{-1}) were purchased from Beijing Biodee Biotechnology Co., Ltd. (Beijing, China). $CdCl_2{\cdot}2.5H_2O$ (99.0%), $NaBH_4$ (96.0%), tellurium powder (99.9%), graphite powder, H_2O_2 (30%), chloroauric acid ($HAuCl_4$), trisodium citrate, and Tween-20 were obtained from Sinopharm Chemical Regent Co. Ltd. (Shanghai, China). (3-Aminopropyl)triethoxysilane (APTS), tetraethoxysilane (TEOS), mercaptopropionic acid (MPA, 99%), bovine serum albumin (BSA), poly(diallyldimethylammonium chloride) (PDDA), N-hydroxysuccinimide (NHS), and 1-ethyl-3-(3-dimethylaminopropyl) carbodiimide hydrochloride (EDC·HCl) were obtained from Sigma-Aldrich Chemicals Co. All other common solvents and salts were of analytical grade and used as received. Phosphate buffered saline (PBS) were prepared by mixing PB solutions with 0.9% NaCl. Ultrapure water (Mill-Q, Millipore, 18.2 MΩ resistivity) was used throughout the experiments.

Apparatus. ECL studies were performed using a Model MPI-EII from ECL Analyzer Systems (Xi'an Remex Electronic Science & Technology Co. Ltd., China). All ECL experiments were performed in a 5 mL glass cell with a conventional three-electrode system composed of a platinum wire as the auxiliary electrode and an Ag/AgCl (saturated KCl) electrode as the reference electrode; working electrodes were bare or modified glass carbon electrodes (GCE, 3 mm diameter). The ECL spectra were measured by placing a series of band-pass filters (bandwidth, 10 nm) of 600, 630, 650, 670, 700, 730, 750, 770, and 800 nm (provided by Beijing Institute of Biophysics, Academia Sinica, China) before the photomultiplier tube (PMT) window and detecting the intensities of ECL passing through these filters under the same experimental conditions respectively. Electrochemical impedance spectroscopy (EIS) analyses were performed with a CHI 660B electrochemical workstation (CH Instrument Co. Shanghai) in the solution of

dx.doi.org/10.1021/ac300498v | *Anal. Chem.* 2012, 84, 4893−4899

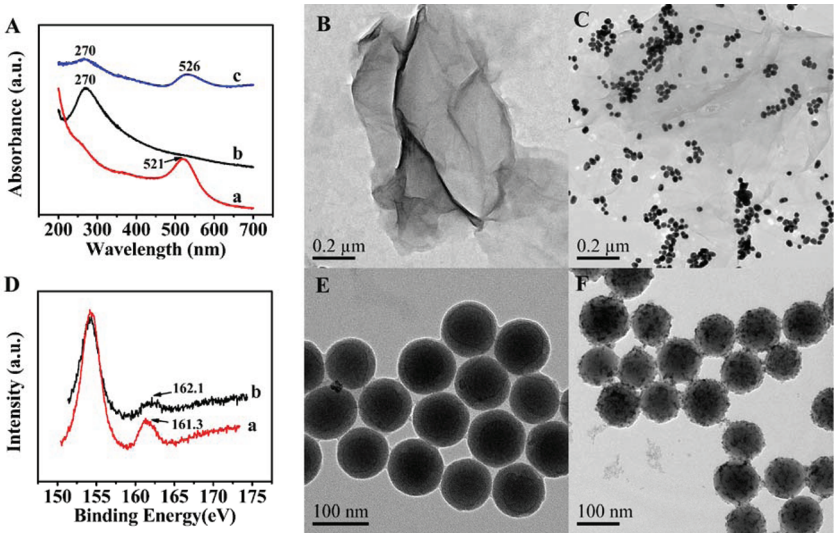

Figure 1. (A) UV−vis absorption spectra of (a) AuNPs, (b) PDDA-GN, and (c) Au-GN hybrids. TEM images of (B) PDDA-GN and (C) Au-GN hybrids. (D) XPS of S2p of (a) SiO_2-QD and (b) SiO_2-QD-Ab2 nanoparticles. TEM images of (E) SiO_2 and (F) SiO_2-QD.

0.10 M KNO_3 containing 20.0 mM $K_3[Fe(CN)_6]/K_4[Fe(CN)_6]$, using the same three-electrode system as in the ECL detection.

UV−vis spectra were acquired on the Nicolet Evolution 300 UV−vis spectrometer coupled with a 1.00 cm quartz cell. Photoluminescence (PL) spectra were performed on an Edinburgh FLS920 spectrometer with an integrating-sphere attachment under excitation of 370 nm. Fourier-transform infrared (FT-IR) spectra were collected on a Nicolet Avatar-330 spectrometer with 4 cm^{-1} resolution using the KBr pellet technique. Raman spectra were recorded by a Renishaw inVia Raman spectrometer equipped with a He−Ne laser excitation source operating at 633 nm. Fluorescence microscopy images were carried out with inverted fluorescence microscope (Eclipse Ti, Nikon). X-ray photoelectron spectroscopy (XPS) was measured by a Thermo VG Multilab 2000 spectrometer equipped with a monochromatic Al Kα radiation source at room temperature. Transmission electron microscopy (TEM) and high-resolution TEM images were acquired using a FEI Tecnai G20 transmission electron microscope operating at an acceleration voltage of 200 kV.

Preparation of the Au-GN Hybrids and SiO_2-QD-Ab2 Labels. The AuNPs, PDDA-capped graphene nanosheets (PDDA-GN), SiO_2 nanospheres, and NIR-emitting CdTe/CdS $core_{small}/shell_{thick}$ QDs were synthesized according to the as-reported methods.[11a,12] The detail information of the preparation of Au-GN hybrids and CdTe/CdS $core_{small}/shell_{thick}$ QDs tagged silica nanosphere immunological labels (SiO_2-QD-Ab2) was shown in the Supporting Information.

Fabrication of the ECL Immunosensor. Prior to each measurement, the GCE with a diameter of 3 mm was successively polished using 1, 0.3, and 0.05 μm alumina slurry and then washed ultrasonically in ethanol and water for 5 min, respectively. The cleaned GCE was dried with high-purity nitrogen steam for the next modification. Six μL of Au-GN hybrid solution was dropped on the center of the pretreated GCE and allowed to dry at room temperature for over 3 h. Then the modified electrode was washed with PBST (PBS with 0.05% Tween, pH 7.4) for at least 15 min to remove unabsorbed materials and immediately incubated with 60 μL of 0.1 mg mL^{-1} Ab1 solution (10 mM PBS, pH 7.4) for 12 h at 4 °C. Next, they were rinsed with PBST to remove physically absorbed Ab1 and blocked with 60 μL 2% BSA solution for 1 h at 37 °C to block possible remaining active sites against nonspecific adsorption. After washing thoroughly with PBST, the Ab1 modified electrode was incubated with 60 μL of the target HIgG samples for 50 min at 37 °C and washed with PBST. Finally, the electrode was incubated with 100 μL of SiO_2-QD-Ab2 labels for 50 min at 37 °C and then washed thoroughly with PBST to remove nonspecifically bounded conjugates.

Standard Procedures for NIR ECL Detection in Aqueous Buffer. In a typical ECL assay in aqueous buffer, the immunosensors with different concentrations of HIgG were used in 0.1 M PBS (pH 7.4) containing 0.1 M $K_2S_2O_8$ and 0.1 M KCl, scanning from 0 V to −1.5 V with a scan rate of 200 mV s^{-1}. The ECL signals were recorded with a Model MPI-EII ECL Analyzer by placing a band-pass filter of 710 nm (bandwidth, 40 nm) before the PMT window and detecting the intensities of ECL passing of emission wavelength between 670 and 750 nm. The emission window was placed in front of the PMT at 850 V.

HIgG Detection in Serum Samples. For the preparation of serum, 10 mL of human blood (provided by Affiliated Hospital, Huazhong Agricultural University) from a healthy man was collected in a sample tube. The serum was separated after putting the sample in an incubator at 37 °C for 30 min for removing red cell. The above serum layer was centrifuged at 1100 r.p.m for 6 min. The resultant human serum sample was then stored at −70 °C until used. For the detection in serum matrix, newly obtained three independent serum samples were 10^9-fold diluted with PBS (0.1 M, pH 7.4), which were then used as the assay medium. The subsequent ECL measurement procedures were the same as above.

RESULTS AND DISCUSSION

Characterization of the Au-GN Hybrids and SiO_2-QD-Ab2 Labels. FT-IR spectra was first employed to investigate the reduction and functionalization process of GN. As can be seen from the Figure S1 (Supporting Information), the dramatical decrease or disappearance of the adsorption bands of oxo-groups on the PDDA-GN indicated that the exfoliated

dx.doi.org/10.1021/ac300498v | Anal. Chem. 2012, 84, 4893−4899

graphite oxide (EGO) had been reduced successfully.[13] The absorption bands at 2929 cm^{-1} (CH_n), 1642 cm^{-1} (C═O), and 1461 cm^{-1} (C═C) corresponded to the characteristic bands of PDDA, indicating the functionalization of graphene with PDDA.[14] Raman spectroscopy was also used to characterize carbonaceous materials. As shown in Figure S2 (Supporting Information), the D/G intensity ratio of PDDA-GN increased notably in comparison with that of EGO, indicating an increase in the number of smaller graphitic domains upon reductions.[15] The as-prepared Au-GN hybrids were first confirmed by UV−vis absorption spectrum as displayed in Figure 1A. The citrate-stabilized AuNPs (curve a) appeared a strong characteristic absorption peak at 521 nm caused by surface plasmon resonance. PDDA-GN (curve b) revealed a strong absorption peak at 270 nm which referred $\pi \rightarrow \pi^*$ transitions of aromatic C═C bond indicating the restoration of the π-conjugation network of the GN. After the AuNPs were deposited, the characteristic peak of AuNPs was observed in Au-GN (curve c) at 526 nm which indicated the efficient adsorption of AuNPs onto the nanosheets surface. Additionally, the typical TEM images of GN before (Figure 1B) and after (Figure 1C) being deposited with AuNPs also clearly demonstrated the formation of the nanocomposites. From an overlook image, it was observed that the GN with some corrugation has been decorated with AuNPs with negligible nanoparticle agglomeration.

Coating of the NIR-emitting $core_{small}/shell_{thick}$ CdTe/CdS QDs onto the surface of SiO_2 nanospheres was achieved through an EDC coupling scheme. The coupling process was first demonstrated by the color change under UV illumination (Figure S3−A, Supporting Information), as well as PL spectra (Figure S3−B, Supporting Information). After being coated with CdTe/CdS QDs, the SiO_2 nanospheres showed the same color as CdTe/CdS QDs in water. Furthermore, the SiO_2 nanospheres displayed a PL peak characteristic of the CdTe/CdS QDs. The slight red shift of the PL peak for the CdTe/CdS tagged SiO_2 nanospheres may be attributed to interparticle plasmon coupling caused by nanoparticle clusters.[16] Additionally, representative TEM and high-resolution TEM images exhibited numerous, individual, dark "QD islands" on SiO_2 nanospheres (Figure 1E, F and Figure S4, Supporting Information), which indicated the QDs were distributed homogeneously on the SiO_2 nanosphere surface. Attachment of Ab2 on the CdTe/CdS QDs tagged SiO_2 nanospheres (SiO_2-QD) was characterized with XPS. As shown in Figure 1D, the binding energy of S2p from SiO_2-QD was 161.3 eV, which was lower than the binding energy of SiO_2-QD-Ab2 after Ab2 coupling (162.1 eV). The results revealed that the coordination situation of S from SiO_2-QD was different from that of SiO_2-QD-Ab2. Therefore, the new S2p binding energy could be ascribed to the sulfur from the disulfide bond in protein (164.1 eV).[17] In addition, conjugating with Ab2 on SiO_2-QD resulted in an increase in the relative elemental compositions of carbon, nitrogen, and sulfur and a decrease in the unrelative elemental compositions of silicon, cadmium, and tellurium (Table S1, Supporting Information). All these facts confirmed that Ab2 was successfully linked to the surface of SiO_2-QD.

Characterization of the ECL Immunosensor. For the immunosensor fabrication (Scheme 1), Au-GN hybrids were first deposited on the glass carbon electrode surface for initial antibody immobilization. After blocking with BSA, the antibody-coated electrode was dipped into the HIgG-containing solution for 50 min at 37 °C to capture HIgG antigen through the first immunoreaction. Finally, the SiO_2-QD-Ab2 labels were brought onto the electrode surface after the second immunoreaction. Under the fluorescence microscopy, several dull-red fluorescence spheres were observed on the SiO_2-QD-Ab2/Ag/BSA/Ab1/Au-GN/GCE at a HIgG concentration of 1 ng mL^{-1} (Figure 2A). In control

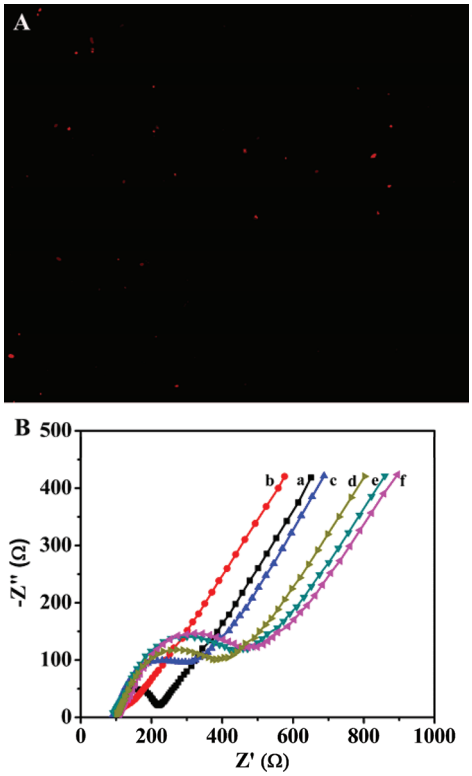

Figure 2. (A) Fluorescence microscope of SiO_2-QD-Ab2/Ag/BSA/Ab1/Au-GN/GCE at a HIgG concentration of 1 ng mL^{-1}. (B) EIS of (a) bare GCE, (b) Au-GN/GCE, (c) Ab1/Au-GN/GCE, (d) BSA/Ab1/Au-GN/GCE, (e) Ag/BSA/Ab1/Au-GN/GCE, and (f) Ab2/Ag/BSA/Ab1/Au-GN/GCE in 0.10 M KNO_3 containing 20.0 mM $K_3[Fe(CN)_6]/K_4[Fe(CN)_6]$.

experiments, there was no fluorescence on either SiO_2-QD-Ab2/BSA/Ab1/Au-GN/GCE or Ag/BSA/Ab1/Au-GN/GCE (Figure S5, Supporting Information). These results confirmed that the captured nanoparticles were from a highly specific immunoassay, and the CdTe/CdS QDs kept their fluorescence properties during the immunoreaction.

EIS is an effective method for monitoring the changes in the surface features of the modified electrodes in the assembly process. The stepwise construction process of the sandwiched immunoassay was further characterized by EIS as shown in Figure 2B. It was observed that the bare GCE revealed a very small semicircular domain (curve a). After the Au-GN film was deposited onto the electrode, the electrode showed a lower resistance (curve b), implying that Au-GN was an excellent electric conducting material and accelerated the electron transfer. Subsequently, the immobilization of Ab1 generated an insulating protein layer (curve c), which increased the resistance. When BSA was assembled onto the composite film (curve d), the electron-transfer resistance increased significantly. Followed by bounding with Ag (curve e), the EIS showed a higher resistance. After the capture of Ab2, the

dx.doi.org/10.1021/ac300498v | Anal. Chem. 2012, 84, 4893−4899

resistance further enlarged. These results were consistent with the fact that the electrode was fabricated as expected.

ECL Spectrum and Detection Window of the Immunosensor. The ECL spectrum of SiO_2-QD-Ab2/Ag/BSA/Ab1/Au-GN/GCE at a HIgG concentration of 1 ng mL^{-1} was recorded by monitoring the intensities of ECL passing through different band-pass filters from 600 to 800 nm (bandwidth, 10 nm) respectively. As displayed in Figure 3A,

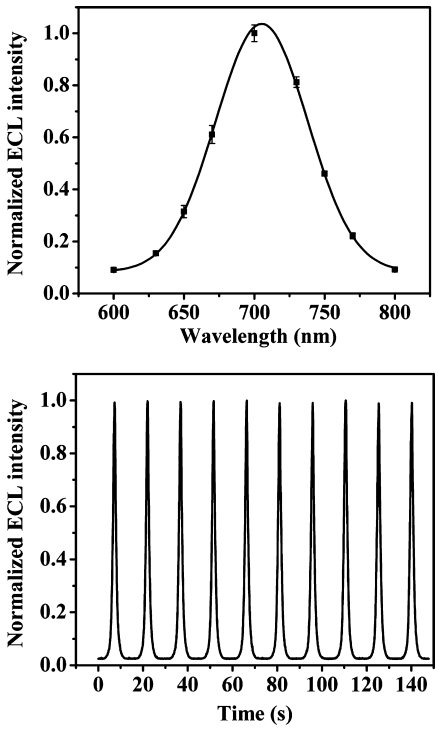

Figure 3. (A) ECL spectrum of the SiO_2-QD-Ab2/Ag/BSA/Ab1/Au-GN/GCE at a HIgG concentration of 1 ng mL^{-1}. (B) ECL emission from SiO_2-QD-Ab2/Ag/BSA/Ab1/Au-GN/GCE under continuous CVs for 10 cycles.

the ECL spectrum of the immunosensor demonstrated a maximum wavelength of around 705 nm, which was almost identical to that in the PL spectrum of the QDs (Figure S3−B, Supporting Information), indicating that the NIR ECL emission was derived from the original NIR-emitting $core_{small}/shell_{thick}$ CdTe/CdS QDs and the novel NIR ECL emitters as synthesized had no deep surface traps causing luminescence at longer wavelength.[3c,d] Most importantly, the phenomenon we observed that the maximum peak of ECL spectrum was slightly lower than that in the PL spectrum of the QDs tagged SiO_2 nanospheres (Figure S3−B, Supporting Information), which suggested the slightly nanoparticle agglomeration on SiO_2 nanosphere surface had no influence to the ECL emission. A control experiment was conducted by detecting the ECL intensity of the immunosensor under the wavelength less than 600 nm (using a short-pass filter before the PTM window). In this situation, no ECL emission was observed (data not shown), confirming the QD-based NIR ECL emission. Thus, the emission wavelength between the 670 and 750 nm was chosen as the ECL detection window for the immunosensor. In this NIR region, interference from biological media such as autofluorescence, scattering light, and absorption for most biomolecules were negligible, which greatly improved the sensitivity for protein sensing in biological samples.[18]

Additionally, the ECL intensities of the immunosensor after dipping in 1 ng mL^{-1} HIgG solution for 50 min remained at a comparatively stable value (1.2% variation) during consecutive cyclic potential scanning (Figure 3B), indicating an acceptable stability for ECL detection.

NIR ECL Detection Using Au-GN Hybrids and SiO_2 Nanospheres for Dual Amplification. The sandwiched immunoassay was also supported by ECL data obtained in the NIR window (670−750 nm). As can be seen ECL intensity−potential curves (Figure 4A), in air-saturated 0.1 M pH 7.4 PBS containing 0.1 M KCl and 0.1 M $K_2S_2O_8$, no obvious increase of ECL emission could be observed on bare GCE (curve a), Ab1/Au-GN/GCE (curve b), Ag/BSA/Ab1/Au-GN/GCE (curve c), SiO_2-QD-Ab2/BSA/Ab1/Au-GN/GCE (curve d), and Ab2/Ag/BSA/Ab1/Au-GN/GCE (curve e), whereas a strong ECL signal appeared from SiO_2-QD-Ab2/Ag/BSA/Ab1/Au-GN/GCE (curve f) at the same HIgG concentration (1 ng mL^{-1}). In a control experiment, there was no ECL emission from the SiO_2-QD-Ab2/Ag/BSA/Ab1/Au-GN/GCE without the presence of 0.1 M $K_2S_2O_8$ (data not shown). The inset showed the cyclic voltammetry (CV) of SiO_2-QD-Ab2/Ag/BSA/Ab1/Au-GN/GCE at a HIgG concentration of 1 ng mL^{-1}, where the peaks at −0.74 and −1.27 V were respectively corresponding to the reduction of $S_2O_8^{2-}$ ions and the CdTe/CdS QDs phase.[8c] It should be noticed that the slight ECL emission (curves a, b, c, d, and e in Figure 4A) was attributed to the reduction of $S_2O_8^{2-}$ ions on the electrode surface. All these results suggested that the enhanced ECL emission was produced by the reaction of the captured SiO_2-QD-Ab2 labels and $S_2O_8^{2-}$. The great amplification of the ECL signal with Au-GN hybrids and SiO_2-QD-Ab2 labels is demonstrated in Figure 4B. Compared with QD-Ab2/Ag/BSA/Ab1/GCE (curve b, CdTe/CdS QDs bound directly with Ab2 and used as the label), the ECL intensity of QD-Ab2/Ag/BSA/Ab1/Au-GN/GCE (curve c) and SiO_2-QD-Ab2/Ag/BSA/Ab1/Au-GN/GCE (curve d) was highly enhanced 4.2-fold and 16.8-fold, respectively. The reasons may be attributed to combining the advantages of high-binding capability and excellent electrical conductivity of hybrid architecture with an increase of CdTe/CdS QD loading per immunoassay event.[10e,11c]

The immunoreaction time is a significant parameter for the HIgG capture and the specific recognition of SiO_2-QD-Ab2 on the electrode. As time increases, the ECL response increased gradually and reached a plateau after 50 min (Figure S6, Supporting Information), indicating a tendency to complete immunoreaction on the electrode surface. Thus, 50 min was used as the optimal immunoreaction time. The effect of detection solution pH on the ECL signals of the immunosensor is displayed in Figure S7 (Supporting Information). In the examined pH range, the maximum ECL response of the immunosensor occurred when pH was close to 7.6. Taking into account the bioactivity of immunoreagents, a pH 7.4 PBS was recommended for use. The ECL responses of the immunosensor over the temperature range from 20 to 50 °C are shown in Figure S8 (Supporting Information). As shown, the ECL response increased with the increasing incubation temperature and reached a maximum at 40 °C and decreased upon increasing the temperature. To obtain higher efficiency of the immunoreaction, 37 °C was selected for the sandwich-type immunoassay.

On the basis of the optimal condition, the sandwiched immunoassay was applied for the HIgG detection. Figure 4C depicts the ECL profiles for the immunosensor before and after

dx.doi.org/10.1021/ac300498v | Anal. Chem. 2012, 84, 4893−4899

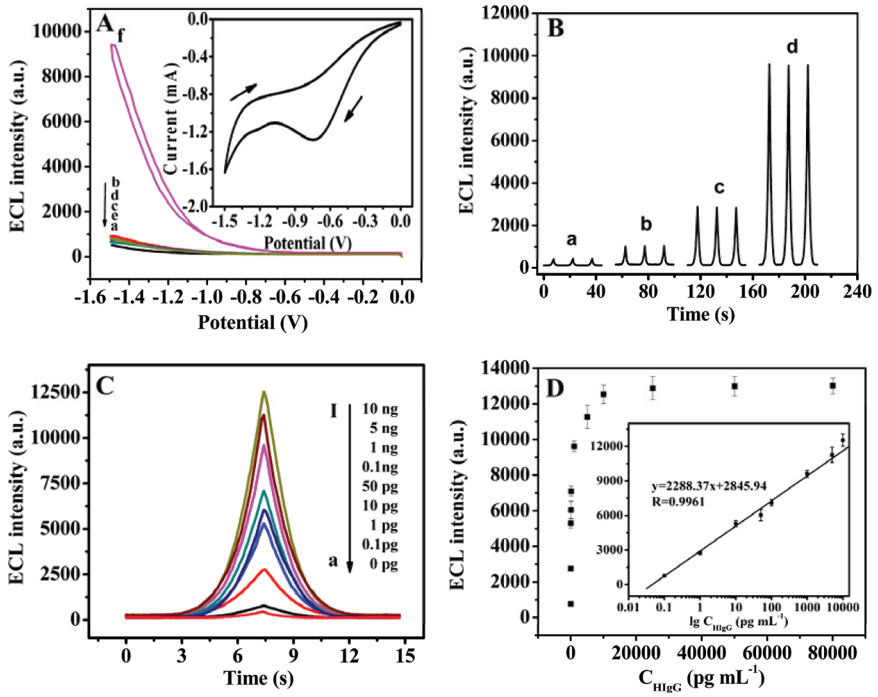

Figure 4. (A) ECL–potential curves obtained at (a) bare GCE, (b) Ab1/Au-GN/GCE, (c) Ag/BSA/Ab1/Au-GN/GCE, (d) SiO_2-QD-Ab2/BSA/Ab1/Au-GN/GCE, (e) Ab2/Ag/BSA/Ab1/Au-GN/GCE, and (f) SiO_2-QD-Ab2/Ag/BSA/Ab1/Au-GN/GCE at the HIgG concentration of 1 ng mL^{-1}. The inset was CV of SiO_2-QD-Ab2/Ag/BSA/Ab1/Au-GN/GCE at the HIgG concentration of 1 ng mL^{-1}. (B) ECL responses of (a) bare GCE, (b) QD-Ab2/Ag/BSA/Ab1/GCE, (c) QD-Ab2/Ag/BSA/Ab1/Au-GN/GCE, and (d) SiO_2-QD-Ab2/Ag/BSA/Ab1/Au-GN/GCE at the HIgG concentration of 1 ng mL^{-1}. (C) ECL profiles of the immunosensor in different concentrations of HIgG (pg mL^{-1}) (a) 0, (b) 0.1, (c) 1, (d) 10, (e) 50, (f) 100, (g) 1000, (h) 5000, (i) 10000 in 0.1 M pH 7.4 PBS containing 0.1 M $K_2S_2O_8$ and 0.1 M KCl, scanning from 0 V to −1.5 V with a scan rate of 200 mV s^{-1}. (D) Calibration curve for HIgG determination.

Table 1. Direct Determination of HIgG Content in Three Human Serum Samples Using the Proposed Immunosensor

sample	measured HIgG concentration (pg mL^{-1})	added HIgG concentration (pg mL^{-1})	found total HIgG concentration (pg mL^{-1})	recovery	RSD (n = 5)
1	10.21	5.00	14.40	83.8%	5.3%
2	9.74	15.00	27.83	120.6%	4.6%
3	11.83	25.00	39.15	109.3%	3.9%

reacting with different concentrations of HIgG. As can be seen, the ECL signal increased with increasing concentrations of HIgG as a consequence of the efficient capture of the HIgG by sandwich immunoassay. The results suggested that the HIgG concentration could be determined with the ECL immunosensor. The standard calibration curve for HIgG detection is illustrated in Figure 4D. The ECL signal increased linearly with the logarithm of HIgG concentrations in the range from 0.1 pg mL^{-1} to 10 ng mL^{-1} (R = 0.9961), and the detection limit was 87 fg mL^{-1} with a signal-to-noise ratio of 3. According to the linear equation, we could detect HIgG concentration quantitatively. Higher HIgG levels could be detected by an appropriate dilution with pH 7.4 PBS. Furthermore, a comparison of the proposed immunosensor with some other immunoassays for the determination of HIgG is made as shown in Table S2 (Supporting Information). The results showed that the present immunosensor had a better performance than some earlier reported methods, especially the detection limit. In particular, compared with other ECL immunosensor in the visible range, the fabricated immunosensor displayed a wider linear detection range and lower detection limit.[5b,19]

Specificity, Reproducibility, and Stability of the Immunosensor. The specificity of the immunosensor played an important role in analyzing biological samples *in situ* without separation. Some coexisting species including BSA (100 ng mL^{-1}), hemoglobulin (100 ng mL^{-1}), glutamic acid (Glu, 100 ng mL^{-1}), L-cysteine (L-Cys, 100 ng mL^{-1}), and glucose (100 ng mL^{-1}) were used as the influences to assess the specificity. The immunosensor was incubated in two copies of 1 ng mL^{-1} HIgG aqueous solutions with and without each of the substances, respectively. No significant difference (RSD = 4.6%) was observed in ECL response from the solution pair, suggesting the acceptable specificity of the immunosensor for HIgG. Reproducibility of the immunosensor for HIgG was investigated with intra- and interassay precision. The intra-assay precision was evaluated by assaying one HIgG level for five similar measurements. The interassay precision was estimated by testing one HIgG level with five immunosensors made at the same electrode independently. The intra- and interassay variation coefficients obtained from 1 ng mL^{-1} HIgG were 4.5% and 6.9%, respectively. This fact demonstrated the immunosensor possessed acceptable reproducibility. Furthermore, we found that the immunosensor retained 93.5% of original ECL response after 15 days of storage in 0.01 M PBS at 4 °C, indicating the good stability of the immunosensor.

HIgG Sensing in Human Serum. To further investigate the feasibility of the immunosensor for the clinical applications, the sensing of HIgG in human serum was carried out. Before

dx.doi.org/10.1021/ac300498v | *Anal. Chem.* 2012, 84, 4893−4899

the determination, the samples were diluted appropriately step by step to be in the linear range of the immunosensor. Table 1 describes the results of three independent serum samples obtained using the proposed immunosensor. It was clearly observed that the concentrations of HIgG were tested as 10.21, 9.74, and 11.83 mg mL^{-1} in undiluted samples, respectively, which fell in the normal range of total HIgG level in human serum. Furthermore, recovery experiments were conducted to validate the determination. It was found that the recoveries were in the range of 83.8−120.6% (Table 1), which was satisfactory for quantitative assays performed in biological samples.

CONCLUSIONS

With the Au-GN hybrids and functionalized SiO_2 nanospheres for signal amplification, a QD-based NIR ECL immunosensor was developed for the first time. The aim of this work was to explore the feasibility of ECL sensing in the NIR region and achieve an accurate analysis of protein in biological samples by taking advantage of lower background interference in NIR window. It has been demonstrated here the immunosensor could be applied to the direct detection of HIgG in both aqueous buffers and the serum samples and exhibited a wider linear detection range with lower detection limit in comparison to the reported ECL immunosensor for HIgG in the visible range. Due to the low PL QY of NIR-emitting QDs and intrinsically low signal-to-noise ratio of PL analytical technique, this proposed immunosensor also provided a promising alternative for QD-based NIR PL sensing strategy. In particular, our sensing strategy would open new avenues on the design of QD-based ECL sensors and intrigue researchers into gaining a new interest in the development of NIR ECL biosensors.

ASSOCIATED CONTENT

Supporting Information

Experimental details, Figures S1−S8, Tables S1 and S2, and references. This material is available free of charge via the Internet at http://pubs.acs.org.

AUTHOR INFORMATION

Corresponding Author

*Phone: +86-27-87288246. Fax: +86-27-87288246. E-mail: hyhan@mail.hzau.edu.cn.

Notes

The authors declare no competing financial interest.

ACKNOWLEDGMENTS

We gratefully acknowledge the financial support from National Natural Science Foundation of China (20975042, 21175051), the Fundamental Research Funds for the Central Universities (2010PY009, 2010PY139, 2010YB03), and the Natural Science Foundation of Hubei Province Innovation Team (2011CDA115).

REFERENCES

(1) (a) Smith, A. M.; Mancini, M. C.; Nie, S. *Nat. Nanotechnol.* **2009**, *4*, 710−711. (b) Ma, Q.; Su, X. *Analyst* **2010**, *135*, 1867−1877.

(2) (a) Zhang, Y.; Li, Y.; Yan, X. P. *Anal. Chem.* **2009**, *81*, 5001−5007. (b) Liang, G. X.; Pan, H. C.; Li, Y.; Jiang, L. P.; Zhang, J. R.; Zhu, J. J. *Biosens. Bioelectron.* **2009**, *24*, 3693−3697. (c) Kim, S.; Lim, Y. T.; Soltesz, E. G.; De Grand, A. M.; Lee, J.; Nakayama, A.; Parker, J. A.; Mihaljevic, T.; Laurence, R. G.; Dor, D. M. *Nat. Biotechnol.* **2003**, *22*, 93−97. (d) He, Y.; Zhong, Y.; Su, Y.; Lu, Y.; Jiang, Z.; Peng, F.; Xu, T.; Su, S.; Huang, Q.; Fan, C. *Angew. Chem., Int. Ed.* **2011**, *50*, 5695−5698.

(3) (a) Ding, Z.; Quinn, B. M.; Haram, S. K.; Pell, L. E.; Korgel, B. A.; Bard, A. J. *Science* **2002**, *296*, 1293−1297. (b) Myung, N.; Ding, Z.; Bard, A. J. *Nano Lett.* **2002**, *2*, 1315−1319. (c) Myung, N.; Bae, Y.; Bard, A. J. *Nano Lett.* **2003**, *3*, 1053−1055. (d) Bae, Y.; Myung, N.; Bard, A. J. *Nano Lett.* **2004**, *4*, 1153−1161.

(4) (a) Ding, S. N.; Xu, J. J.; Chen, H. Y. *Chem. Commun.* **2006**, 3631−3633. (b) Wang, X. F.; Xu, J. J.; Chen, H. Y. *J. Phys. Chem. C* **2008**, *112*, 7151−7157.

(5) (a) Jie, G.; Liu, B.; Pan, H.; Zhu, J. J.; Chen, H. Y. *Anal. Chem.* **2007**, *79*, 5574−5581. (b) Jie, G.; Zhang, J.; Wang, D.; Cheng, C.; Chen, H. Y.; Zhu, J. J. *Anal. Chem.* **2008**, *80*, 4033−4039.

(6) (a) Zou, G.; Ju, H. *Anal. Chem.* **2004**, *76*, 6871−6876. (b) Han, H. Y.; Sheng, Z. G.; Liang, J. G. *Anal. Chim. Acta* **2007**, *596*, 73−78.

(7) Jiang, H.; Ju, H. *Chem. Commun.* **2007**, 404−406.

(8) (a) Sun, L.; Bao, L.; Hyun, B. R.; Bartnik, A. C.; Zhong, Y. W.; Reed, J. C.; Pang, D. W.; Abruña, H. C. D.; Malliaras, G. G.; Wise, F. W. *Nano Lett.* **2008**, *9*, 789−793. (b) Liang, G. X.; Li, L. L.; Liu, H. Y.; Zhang, J. R.; Burda, C.; Zhu, J. J. *Chem. Commun.* **2010**, *46*, 2974−2976. (c) Wang, J.; Jiang, X. C.; Han, H. Y.; Li, N. *Electrochem. Commun.* **2011**, *13*, 359−362. (d) Zou, G. Z.; Liang, G. D.; Zhang, X. L. *Chem. Commun.* **2011**, *47*, 10115−10117. (e) Liang, G.; Shen, L.; Zou, G.; Zhang, X. *Chem.—Eur. J.* **2011**, *17*, 10213−10215.

(9) (a) Stankovich, S.; Dikin, D. A.; Dommett, G. H. B.; Kohlhaas, K. M.; Zimney, E. J.; Stach, E. A.; Piner, R. D.; Nguyen, S. T.; Ruoff, R. S. *Nature* **2006**, *442*, 282−286. (b) Li, D.; Kaner, R. B. *Science* **2008**, *320*, 1170−1171. (c) Geim, A. K.; Novoselov, K. S. *Nat. Mater.* **2007**, *6*, 183−191.

(10) (a) Xu, C.; Wang, X.; Zhu, J. *J. Phys. Chem. C* **2008**, *112*, 19841−19845. (b) Liu, J.; Fu, S.; Yuan, B.; Li, Y.; Deng, Z. *J. Am. Chem. Soc.* **2010**, *132*, 7279−7281. (c) Hong, W.; Bai, H.; Xu, Y.; Yao, Z.; Gu, Z.; Shi, G. *J. Phys. Chem. C* **2010**, *114*, 1822−1826. (d) Fang, Y.; Guo, S.; Zhu, C.; Zhai, Y.; Wang, E. *Langmuir* **2010**, *26*, 11277−11282. (e) Liu, K. P.; Zhang, J. J.; Wang, C. M.; Zhu, J. J. *Biosens. Bioelectron.* **2011**, *26*, 3627−3632.

(11) (a) Wu, Y.; Chen, C.; Liu, S. *Anal. Chem.* **2009**, *81*, 1600−1607. (b) Chen, L. Y.; Chen, C. L.; Li, R. N.; Li, Y.; Liu, S. Q. *Chem. Commun.* **2009**, 2670−2672. (c) Qian, J.; Zhang, C.; Cao, X.; Liu, S. *Anal. Chem.* **2010**, *82*, 6422−6429. (d) Yuan, L.; Hua, X.; Wu, Y.; Pan, X.; Liu, S. *Anal. Chem.* **2011**, *83*, 6800−6809.

(12) (a) Frens, G. *Nature* **1973**, *241*, 20−22. (b) Kovtyukhova, N. I.; Ollivier, P. J.; Martin, B. R.; Mallouk, T. E.; Chizhik, S. A.; Buzaneva, E. V.; Gorchinskiy, A. D. *Chem. Mater.* **1999**, *11*, 771−778. (c) Liu, K. P.; Zhang, J. J.; Yang, G. H.; Wang, C. M.; Zhu, J. J. *Electrochem. Commun.* **2010**, *12*, 402−405. (d) Deng, Z.; Schulz, O.; Lin, S.; Ding, B.; Liu, X.; Wei, X.; Ros, R.; Yan, H.; Liu, Y. *J. Am. Chem. Soc.* **2010**, *132*, 5592−5593.

(13) (a) Shan, C.; Yang, H.; Han, D.; Zhang, Q.; Ivaska, A.; Niu, L. *Langmuir* **2009**, *25*, 12030−12033. (b) Zhang, H.; Lv, X.; Li, Y.; Wang, Y.; Li, J. *ACS Nano* **2009**, *4*, 380−386.

(14) Yang, D. Q.; Rochette, J. F.; Sacher, E. *J. Phys. Chem. B* **2005**, *109*, 4481−4484.

(15) Liang, J.; Chen, Z.; Guo, L.; Li, L. *Chem. Commun.* **2011**, *47*, 5476−5478.

(16) Dong, H.; Yan, F.; Ji, H.; Wong, D. K. Y.; Ju, H. *Adv. Funct. Mater.* **2010**, *20*, 1173−1179.

(17) Hansen, A. G.; Boisen, A.; Nielsen, J. U.; Wackerbarth, H.; Chorkendorff, I.; Andersen, J. E. T.; Zhang, J.; Ulstrup, J. *Langmuir* **2003**, *19*, 3419−3427.

(18) Thomas, J.; Sherman, D. B.; Amiss, T. J.; Andaluz, S. A.; Pitner, J. B. *Bioconjugate Chem.* **2007**, *18*, 1841−1846.

(19) (a) Qi, H.; Zhang, Y.; Peng, Y.; Zhang, C. *Talanta* **2008**, *75*, 684−690. (b) Tian, D.; Duan, C.; Wang, W.; Li, N.; Zhang, H.; Cui, H.; Lu, Y. *Talanta* **2009**, *78*, 399−404. (c) Tian, D.; Duan, C.; Wang, W.; Cui, H. *Biosens. Bioelectron.* **2010**, *25*, 2290−2295. (d) Wu, A. H.; Sun, J. J.; Fang, Y. M.; Su, X. L.; Chen, G. N. *Talanta* **2010**, *82*, 1455−1461.